This is an open access article published under an ACS AuthorChoice License, which permits copying and redistribution of the article or any adaptations for non-commercial purposes.

THE JOURNAL OF PHYSICAL CHEMISTRY B

Article

pubs.acs.org/JPCB

Time Scales of Conformational Gating in a Lipid-Binding Protein

Shuji Kaieda* and Bertil Halle*

Department of Biophysical Chemistry, Lund University, P.O. Box 124, SE-22100 Lund, Sweden

Supporting Information

ABSTRACT: Lipid-binding proteins sequester amphiphilic molecules in a large internal cavity occupied by ∼30 water molecules, some of which are displaced by the ligand. The role of these internal water molecules in lipid binding and release is not understood. We use magnetic relaxation dispersion (MRD) to directly monitor internal-water dynamics in apo and palmitate-bound rat intestinal fatty acid-binding protein (rIFABP). Specifically, we record the water ^{2}H and ^{17}O MRD profiles of the apo and holo forms of rIFABP in solution or immobilized by covalent cross-links. A global analysis of this extensive data set identifies three internal-water classes with mean survival times of ∼1 ns, ∼100 ns, and ∼6 μs. We associate the two longer time scales with conformational fluctuations of the gap between β-strands D and E (∼6 μs) and of the portal at the helix-capped end of the β-barrel (∼100 ns). These fluctuations limit the exchange rates of a few highly ordered structural water molecules but not the dissociation rate of the fatty acid. The remaining 90% (apo) or 70% (holo) of cavity waters exchange among internal hydration sites on a time scale of ∼1 ns but exhibit substantial orientational order, particularly in the holo form.

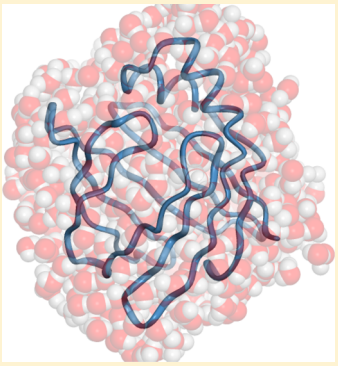

1. INTRODUCTION

Lipid-binding proteins (LBPs) are involved in the intracellular uptake and trafficking of marginally soluble lipids and in the regulation of lipid metabolism and lipid-dependent cell response.[1−3] Despite a modest sequence homology of 20−70%, the LBPs have a highly conserved[4] tertiary structure: a 10-stranded β-barrel (βA−βJ) capped by two short α-helices (α1 and α2), enclosing a large hydrated cavity that harbors the lipid binding site.[5−10] The apo (ligand-free) and holo (ligand-bound) forms of most LBPs have nearly identical mean structures (Figure 1), with no cavity opening large enough to allow the lipid to pass through. Lipid binding and release must therefore be conformationally gated, but the mechanism of this process remains poorly understood. Key to further progress is a detailed characterization of the relevant conformational fluctuations and the role played by the cavity water.

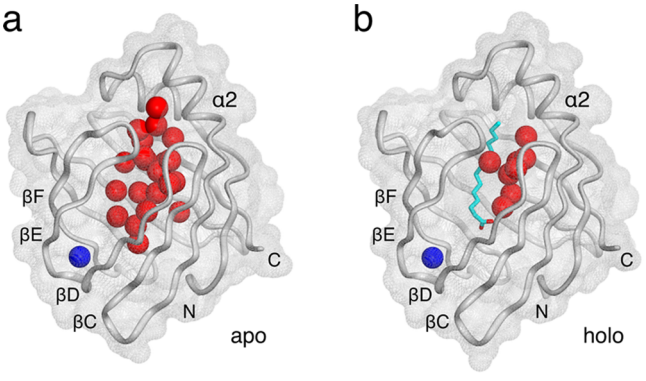

Figure 1. Crystal structures of (a) apo-rIFABP (PDB ID: 1IFC[6]) and (b) myristate-rIFABP (1ICM[8]). Proteins are shown in tube and surface representations, and the ligand is shown in stick representation. The spheres represent crystallographically identified internal water molecules in the ligand-binding cavity (red) and in a distinct small cavity (blue), denoted w135. The figure was prepared with CueMol (http://www.cuemol.org).

Crystal structures of rat intestinal fatty acid-binding protein (rIFABP) suggested[5] that the fatty acid (FA) enters and leaves via a "portal" region, delimited by the α2-helix and the βC−βD and βE−βF loops (at the "top" of the structures in Figure 1). This hypothesis is supported by NMR observations of conformational disorder in the portal region of apo-rIFABP[10] and of faster FA dissociation from an rIFABP variant lacking the two α-helices.[11] Furthermore, the α-helices of rIFABP have been shown to interact directly with phospholipid membranes, indicating that the portal mediates lipid transfer.[12−14] But molecular dynamics (MD) simulations of rIFABP[14] and other LBPs[15−17] have raised the possibility that the portal may not be the only way for lipids to enter and leave the binding cavity.

The dissociation rate of FAs (oleate and linoleate) bound to rIFABP is ∼3 s^{-1} at 25 °C.[18] If the portal is modeled as a gate that can exist in open and closed states, then the FA dissociation rate is a lower bound on the opening rate. If the opening rate is much faster than 3 s^{-1}, as seems likely, then it is not rate-limiting, and the FA dissociation rate is proportional to the open-state probability. Indeed, an NMR study of human liver FABP concluded that the functionally relevant conformational fluctuations in the portal region occur on the microsecond, or even submicrosecond, time scale at 20 °C,

Received: April 2, 2015
Revised: May 21, 2015
Published: May 27, 2015

© 2015 American Chemical Society

DOI: 10.1021/acs.jpcb.5b03214
J. Phys. Chem. B 2015, 119, 7957−7967

making them inaccessible by conventional NMR relaxation experiments.[19]

Another key aspect of LBP function is the water within the binding cavity. Crystal structures model 22 water molecules in the binding cavity of apo-rIFABP,[6] 6 in palmitate-rIFABP,[5] and 8 in myristate-rIFABP[8] (Figure 1). However, MD simulations[20,21] indicate that the binding cavity also contains positionally disordered water molecules that are not detected by X-ray diffraction. In addition to the large water cluster in the binding cavity, the β-barrel contains a water molecule buried in a separate small cavity near the βD−βE loop (Figure 1).[22] Highly conserved within the LBP family,[22,23] this structural water molecule (denoted w135 in the apo-rIFABP structure 1IFC) is believed to play a decisive role in the folding mechanism.[24,25]

The cavity water molecules are not only an essential part of the FA binding thermodynamics; their exchange with external water can also provide important clues about the FA binding mechanism. The dynamics of the internal water molecules in rIFABP have been studied by ^{2}H and ^{17}O magnetic relaxation dispersion (MRD) experiments[26,27] and by MD simulations.[20,21,28] Unlike most other proteins, LBPs yield MRD profiles with a prominent high-frequency dispersion, corresponding to a correlation time of ∼1 ns, in addition to the usual dispersion step from long-lived water molecules that tumble with the protein.[26,27] This finding was first interpreted in terms of two classes of internal water molecules with different mean survival times (MSTs).[26] (The MST is sometimes referred to as the residence or exchange time.) A subsequent MRD study favored an interpretation where the 1 ns correlation time reflects water exchange among intracavity hydration sites, while conformationally gated exchange with external water occurs on a much longer time scale.[27] Relatively short (1−5 ns) MD simulations of rIFABP[20,21,28] recorded multiple water exchanges between the cavity and external solvent via the portal region as well as via a "gap" between strands βD and βE and via a "backside portal" at the opposite end of the β-barrel from the portal (near the N terminus).

Our focus here is on the slower water exchange that may be gated by conformational fluctuations that also enable FA exchange. The MD trajectories analyzed so far[20,28] are too short to access the time scale of the slowest internal-water exchange in rIFABP, for which the MRD data provide rigorous lower and upper bounds of ∼10 ns and several μs, respectively.[26,27] A 100 ns MD simulation[29] of another LBP (chicken liver bile acid-binding protein) found that only one water molecule remains in the apo cavity throughout the trajectory, whereas seven water molecules remain in the holo cavity where the portal is blocked by one of the two bound cholate molecules.[30] Neither for these water molecules (with MST ≫ 100 ns) nor for the handful of water molecules that were observed to exchange once or twice during the trajectory could a statistically meaningful MST be determined. Water exchange pathways and intracavity exchange were not analyzed in this study. Recently, MD trajectories of 210 and 150 ns were reported for the apo and holo forms, respectively, of human heart-type FABP at 310 K.[31] The apo form was found to alternate between a closed and an open conformation and extensive water exchange was observed through the portal and gap, but MST statistics were not reported.[31]

MRD experiments on solutions of freely tumbling proteins provide the product $N\mathcal{S}^2$ of the number N of "long-lived" internal water molecules (with MST τ_S exceeding the protein's tumbling time τ_R) and their mean-square orientational order parameter $\mathcal{S}^2$.[32,33] Typically, the correlation time τ_C extracted from the MRD profile equals the expected τ_R, in which case it can only be concluded that $\tau_R \ll \tau_S \ll (\omega_Q^2\, \mathcal{S}^2\, \tau_R)^{-1}$, where ω_Q is the nuclear quadrupole frequency.[32,33] As noted above, this leads to lower and upper bounds on the MST of ∼10 ns and several μs. The two previous MRD studies of LBPs only examined protein solutions and could therefore not determine MSTs longer than ∼10 ns.[26,27]

More precise information about the MST can be obtained from MRD experiments on protein gels, where protein tumbling is quenched by covalent cross-links.[34,35] Spin relaxation is then induced directly by water exchange, rather than by protein rotational diffusion, a relaxation mechanism known as exchange-mediated orientational randomization (EMOR).[36,37] For the quadrupolar water nuclides ^{2}H and ^{17}O, a general (nonperturbative) spin relaxation theory is available that allows MSTs up to ∼10 μs to be determined if the MRD profile is recorded over a wide frequency range.[36,37] Here, we use this approach to study water exchange from the binding cavity of apo-rIFABP and palmitate-rIFABP. An extensive set of ^{2}H and ^{17}O MRD data, recorded on protein gels as well as on protein solutions, allows us to dissect the complex dynamic behavior of cavity water in rIFABP. Notably, we find dominant dispersion components with MSTs of ∼6 μs and 110−140 ns at 27 °C, which we attribute to conformational gating in the gap and portal regions, respectively.

2. MATERIALS AND METHODS

2.1. Sample Preparation. The gene encoding rIFABP was codon-optimized for expression by *Escherichia coli*, synthesized by DNA2.0 (Menlo Park, CA), and inserted into the pNIC28-Bsa4 plasmid.[38] The expression vector yields rIFABP fusioned with a His_6 tag and the tobacco etch virus (TEV) protease cleavage site at the N terminus. The protein was expressed using *E. coli* TUNER(DE3) strain (Novagen) in Terrific Broth (Difco). After harvesting, the bacterial cells were resuspended in a lysis buffer (50 mM sodium phosphate, 300 mM NaCl, 10 mM imidazole, pH 8.0) and homogenized by French press. The cell lysate was ultracentrifuged, and the supernatant was purified by affinity chromatography (HisTrap; GE Healthcare). To cleave off the His_6 tag, the rIFABP fusion protein was mixed with His_6-tagged TEV protease. The His_6 tag and the protease were then removed by passing the solution through the HisTrap column. Thus, purified rIFABP was delipidated on a Lipidex-1000 (PerkinElmer) column, followed by dialysis against Milli-Q water and freeze drying. Protein purity was verified by mass spectrometry, complete amino acid analysis, and sodium dodecyl sulfate polyacrylamide gel electrophoresis (>95%).

NMR samples of apo-rIFABP were prepared by dissolving the lyophilized, delipidated protein in ^{17}O-enriched D_2O (99.9% ^{2}H, 10.9% ^{17}O, 12.4% ^{18}O) containing 20 mM sodium phosphate buffer (pD 7.4). To prepare holo-rIFABP, a chloroform solution of palmitic acid (PA; Sigma-Aldrich) in a glass vial was exposed to a stream of argon to evaporate the solvent. A solution of apo-rIFABP was then added to the PA-coated vial and gently stirred at 6 °C for 3−6 days. For solution MRD measurements, the rIFABP solution was transferred to a 10 mm o.d. NMR tube. Protein gels were made by mixing rIFABP solutions with 25% (w/w) glutaraldehyde solution (GA; Sigma-Aldrich) and letting the mixture react overnight at

DOI: 10.1021/acs.jpcb.5b03214
J. Phys. Chem. B 2015, 119, 7957−7967

6 °C in a glass tube (8 mm o.d. × ∼12 mm height), which was then wrapped with parafilm and placed in a 10 mm NMR tube. An aliquot of the reaction mixture was cross-linked in a separate tube to measure the pD of the gels. The protein concentration (Table 1) in each rIFABP solution or gel sample examined by

Table 1. Magnetic Relaxation Dispersion Sample Characteristics[a]

property (unit)	apo solution	holo solution	apo gel	holo gel
[IFABP] (mM)[b]	1.72	1.58	4.56	4.34
(mol GA)/(mol IFABP)			24.8	26.1
pD	7.4	7.4	7.0	6.9
θ_{PA}	0.07	0.47	0.09	0.57

[a]All samples contained 20 mM sodium phosphate buffer. [b]In the figures, all R_1 values were scaled to the same protein concentration (2.15 mM or N_W = 25 000).

MRD was determined by complete amino acid analysis, performed at Amino Acid Analysis Center, Department of Biochemistry and Organic Chemistry, Uppsala University, Sweden.

Our experimental approach relies on the assumption that cross-linking does not significantly perturb the structure or dynamics of the protein. To identify any structural perturbation, we investigated solutions and GA cross-linked gels of rIFABP by small-angle X-ray scattering (SAXS).[39] The agreement of the solution and gel SAXS profiles at high q values[39] (where the structure factor can be set to unity) shows that cross-linking of rIFABP by GA at concentrations similar to the ones used here does not significantly perturb the protein structure. The effect of cross-linking on protein dynamics can be investigated by recording MRD profiles from multiple gel samples with different protein concentration and different GA/protein ratio. This has been done for the proteins BPTI and myoglobin,[34,35] which were available in larger quantities than the protein investigated here. The absence of significant effects on the MRD profile in the range of protein and GA concentrations used here[34,35] provides support, if not rigorous proof, for the assumption of negligible dynamic perturbation.

To quantify the amount of FA in the MRD samples, the lipids were extracted from the rIFABP solutions (before adding GA to the gel samples) with cyclohexane supplemented with a known amount of heptadecanoic acid (HDA; Acros Organics) as an internal standard, followed by addition of HCl to protonate the FAs. Standard samples containing different known amounts of PA as well as a fixed amount of HDA in cyclohexane were also prepared. The solutions of FA in cyclohexane were mixed with 1.5% (v/v) H_2SO_4 in methanol and incubated at 50 °C for 2 h to yield methyl esters. Saturated aqueous NaCl solution and 2% (w/v) aqueous sodium bicarbonate were then added to the reaction mixture and vortexed after each addition. Finally, the methyl esters in the cyclohexane phase of the mixtures were analyzed by gas chromatography (GC) on a Varian 430-GC instrument equipped with a Supelcowax 10 capillary column (60 m × 0.32 mm; Sigma-Aldrich). No lipids other than PA and HDA were detected in the GC analysis (Supporting Information, Figure S1). The PA occupancy θ_{PA} determined in this way is given in Table 1 and Supporting Information, Figure S2. In the following, we refer to the nominal apo-rIFABP samples (with θ_{PA} = 0.07 or 0.09) as "apo" and to the nominal palmitate-rIFABP samples (with θ_{PA} = 0.47 or 0.57) as "holo".

2.2. Nuclear Magnetic Resonance Experiments. Six different NMR setups were used to record the water ^{2}H and ^{17}O longitudinal relaxation rate R_1: (1) a Stelar Spinmaster 1 T fast field-cycling (FC) spectrometer (^{2}H: 1.5 kHz to 5.4 MHz); (2) a Tecmag Apollo spectrometer equipped with a GMW field-variable (≤1.8 T) iron-core magnet (^{2}H: 1.0−1.8 MHz, ^{17}O: 0.9−1.6 MHz); (3) a Tecmag Discovery spectrometer equipped with a Drusch field-variable (≤2.1 T) iron-core magnet (^{2}H: 2.5−13.1 MHz; ^{17}O: 2.2−11.5 MHz) or (4) with a Bruker 4.7 T superconducting magnet (^{2}H: 30.7 MHz; ^{17}O: 27.1 MHz); (5) a Varian DirectDrive 500 spectrometer (^{2}H: 76.7 MHz; ^{17}O: 67.8 MHz); and (6) a Varian DirectDrive 600 spectrometer (^{2}H: 92.1 MHz; ^{17}O: 81.3 MHz). For the ^{2}H FC measurements, prepolarized single-pulse (≤2.6 MHz) or inversion recovery (>2.6 MHz) sequences were used with prepolarization and detection at 5.4 and 4.8 MHz, respectively.[40] On the other spectrometers, standard inversion recovery pulse sequences were used. Experiments were performed at 4.0, 15.0, 27.0, or 35.0 ± 0.1 °C, maintained by a thermostated air flow. The sample temperature was checked by using a thermocouple referenced to an ice−water bath and by recording, at each frequency, the bulk solvent relaxation rate in a reference sample (20 mM sodium phosphate at pD 7.4 in water with 99.9% ^{2}H, 10.9% ^{17}O, and 12.4% ^{18}O).

2.3. Analysis of Magnetic Relaxation Dispersion Data. The frequency dependence of the water ^{2}H and ^{17}O R_1 measured on solutions of freely tumbling rIFABP was described by the standard multicomponent exchange model as[32,33]

$$R_1(\omega_0) = R_1^0 + \frac{1}{N_W}\left[N_H(\xi_H - 1)R_1^0 + \sum_k N_k R_1^k(\omega_0)\right] \quad (1)$$

The known quantities in eq 1 are the Larmor frequency ω_0 (in rad s^{-1}), the frequency-independent relaxation rate R_1^0 of bulk solvent (measured on a reference sample), and the water/protein mole ratio N_W in the sample, computed from the protein concentration and the (partial) volumes of rIFABP (18.8 nm^3) and water. To facilitate comparison, all MRD profiles $R_1(\omega_0)$ presented here were normalized to N_W = 25 000 (corresponding to a protein concentration of 2.15 mM), using the fact that the excess relaxation rate $R_1(\omega_0) - R_1^0$, is inversely proportional to N_W.

The first term within brackets in eq 1 is associated with the external hydration shell, comprising N_H water molecules whose rotation is slowed down, on average, by a factor ξ_H relative to bulk solvent.[41] For rIFABP, N_H = 663 was estimated by dividing the solvent-accessible surface area, 7123 Å^2 (the average for the apo- and holo-rIFABP structures in Figure 1), with the mean surface area, 10.75 Å^2, occupied by one water molecule in the first hydration layer.[41]

The sum in eq 1 runs over kinetically distinct dispersion components that are resolved in the MRD profile $R_1(\omega_0)$. The number N_k of water molecules associated with component k can be nonintegral since hydration sites may be partially occupied. The intrinsic relaxation rate $R_k(\omega_0)$ of component k is described in the model-free approach as[33,42]

$$R_1^k(\omega_0) = \omega_Q^2\, \mathcal{S}_k^2\, \tau_{C,k}\left[\frac{0.2}{1 + (\omega_0\, \tau_{C,k})} + \frac{0.8}{1 + (2\, \omega_0\, \tau_{C,k})}\right] \quad (2)$$

where $\mathcal{S}_k$ is the isotropic orientational order parameter[32,33,42] and ω_Q is the rigid-lattice nuclear quadrupole frequency (8.70

DOI: 10.1021/acs.jpcb.5b03214
J. Phys. Chem. B 2015, 119, 7957−7967

$\times 10^5$ rad s^{-1} for ^{2}H and 7.61 $\times 10^6$ rad s^{-1} for ^{17}O).[32] The correlation time $\tau_{C,k}$ is related to the protein tumbling time τ_R and the mean survival time (MST) $\tau_{S,k}$ of water component k as $\tau_{C,k}^{-1} = \tau_R^{-1} + \tau_{S,k}^{-1}$.[33,42] The contribution to $R_1^k(\omega_0)$ from internal motions in the hydration site, typically on a sub-picosecond time scale, was neglected in eq 2 since $N_k \ll N_H$.

Equation 1 is strictly valid only when the MST in site k is sufficiently short that the fast-exchange condition $R_1^k(0)\tau_{S,k} \ll 1$ is fulfilled. In the dilute regime ($N_W \gg 1$), however, eq 1 remains valid to an excellent approximation even outside the fast-exchange regime, if N_k and $\tau_{C,k}$ in eqs 1 and 2 are reinterpreted as effective parameters given by[32,33]

$$\frac{N_k^{\text{eff}}}{N_k} = \frac{\tau_{C,k}^{\text{eff}}}{\tau_{C,k}} = (1 + \omega_Q^2\, \mathcal{S}_k^2\, \tau_{C,k}\, \tau_{S,k})^{-1/2} \tag{3}$$

MRD profiles from gel samples with immobilized rIFABP were analyzed with the general EMOR theory.[34,37] Since protein tumbling is inhibited by the cross-links, internal water molecules are orientationally randomized by the exchange process itself, meaning that $\tau_{C,k} = \tau_{S,k}$. If water exchange is sufficiently fast that $\omega_Q\, \tau_{S,k} \ll 1$, the conventional perturbation theory of spin relaxation remains valid, and the MRD profile can be described by eq 2 (with $\tau_{C,k} = \tau_{S,k}$). For slower exchange, such that $\omega_Q\, \tau_{S,k} \gtrsim 1$, the general EMOR theory based on the stochastic Liouville equation must be used. For ^{2}H, we computed $R_1(\omega_0)$ numerically from the exact EMOR expression for the dilute regime ($N_W \gg 1$), eq (4.7) of ref 37. For ^{17}O, accurate but approximate analytical expressions are available for $\eta_k = 0$ and $\eta_k = 1$ (T. Nilsson and B. Halle, to be published). Although $R_1^k(\omega_0)$ depends only weakly on η_k, we used the expression for $\eta_k = 1$, which should be more accurate for highly ordered internal water molecules (see below)

$$R_1^k(\omega_0) = \frac{16}{175}\frac{Q_k^2}{\tau_{S,k}}\left[\frac{130}{147}\left(\frac{1}{1 + Q_k^2 + L_k^2} + \frac{4}{1 + Q_k^2 + 4L_k^2}\right) + \frac{17}{147}\left(\frac{1}{1 + 4Q_k^2 + L_k^2} + \frac{4}{1 + 4Q_k^2 + 4L_k^2}\right)\right] \tag{4}$$

where $L_k \equiv \omega_0\, \tau_{S,k}$ and $Q_k^2 \equiv (35/12)(\omega_Q\, S_k\, \tau_{S,k})^2(1 + \eta_0^2/3)^{-1}$.

In the general EMOR theory, each component is described by four parameters, namely, N_k, S_k, η_k, and $\tau_{S,k}$,[34,37] while in eq 2 only two parameters, $N_k\, \mathcal{S}_k^2$ and $\tau_{C,k}$ (or their effective counterparts), are required. The two parameters S_k and η_k are related to the isotropic order parameter as[37]

$$\mathcal{S}_k^2 = S_k^2 \frac{1 + \eta_k^2/3}{1 + \eta_0^2/3} \tag{5}$$

where η_0 is the rigid-lattice asymmetry parameter (0.11 for ^{2}H, 0.93 for ^{17}O).[32] Whereas S_k is the $m = 0$ component of the spherical order tensor, $\mathcal{S}_k$ depends on all tensor components. Both S_k^2 and $\mathcal{S}_k^2$ are confined to the range 0−1. For highly ordered internal water molecules, $S_k^2 \approx \mathcal{S}_k^2 \approx 1$ and $\eta_k \approx \eta_0$. Using eq 5, it can be seen that eq 4 reduces to eq 2 in the fast-exchange (or motional-narrowing) limit, $Q_k^2 \ll 1$.

In fitting these models to the MRD data, we used the trust-region reflective nonlinear optimization algorithm[43] with the parameters constrained to their physically admissible ranges. Quoted parameter uncertainties correspond to one standard deviation (68.3% confidence level) and were determined by the Monte Carlo method with a uniform R_1 error of 0.5% (^{2}H solution data) or 1% (all other data), estimated from the scatter in the frequency-independent reference relaxation rate R_1^0. Because each sample is a mixture of apo and holo forms, the MRD profiles from the nominal apo and holo samples were fitted jointly using the population weighted average

$$R_1(\omega_0) = (1 - \theta_{PA})R_1^{\text{apo}}(\omega_0) + \theta_{PA}\, R_1^{\text{holo}}(\omega_0) \tag{6}$$

We thus obtain one set of parameter values for the apo form and another set for the holo form. However, since the tertiary structure is virtually identical for the two forms,[6,8] some of the model parameters were constrained to the same value for the apo and holo forms.

3. RESULTS

Water ^{2}H and ^{17}O MRD profiles were recorded for the rIFABP samples listed in Table 1. The apo and holo labels are nominal; the actual fractions of the apo and holo forms in the samples were determined by GC. Using these fractions, we performed joint fits to the apo and holo MRD profiles from each sample. Because the ^{2}H and ^{17}O profiles were measured on the same sample (with ^{17}O-enriched D_2O as solvent), the model parameters deduced from the ^{2}H and ^{17}O profiles can be compared directly without correction for solvent isotope effects. For the gel samples, where the dispersion extends over a wide frequency range, we measured the ^{2}H profile over five frequency decades (10^3−10^8 Hz) using the FC technique[40] as well as conventional fixed-field relaxation experiments. The ^{17}O profiles are restricted to two decades (10^6−10^8 Hz), since this nuclide relaxes too rapidly to apply the FC technique. All measurements were performed at 27.0 °C, except for the ^{2}H gel profile, which was also measured at 4.0, 15.0, and 35.0 °C.

3.1. Gel Magnetic Relaxation Dispersion Profiles.

The ^{2}H MRD profiles measured on the two rIFABP gel samples at 27 °C are shown in Figure 2, and the parameter values resulting from a joint fit to these profiles are collected in Table 2. Apart from the ubiquitous frequency-independent excess relaxation (referred to as component 0), three dispersion components (labeled 1−3 in order of increasing MST) are required to adequately describe the MRD data in Figure 2. In the joint fit, the three parameters describing components 0 and 1, which are both associated with the external hydration shell, were assumed

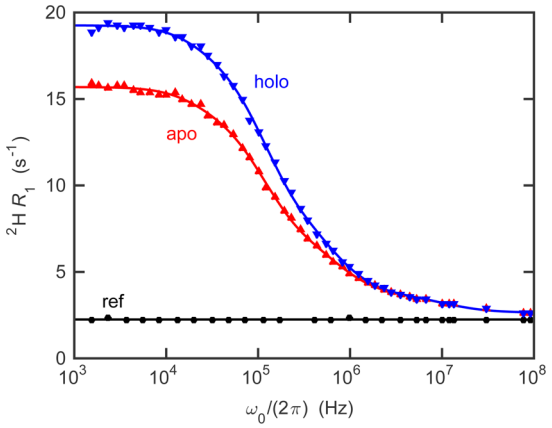

Figure 2. Water ^{2}H MRD profiles from apo (▲) and holo (▼) rIFABP gels at 27.0 °C. Reference sample R_1 values are also shown (●). The two curves resulted from a joint fit to both profiles with the model parameters given in Table 2.

DOI: 10.1021/acs.jpcb.5b03214
J. Phys. Chem. B 2015, 119, 7957−7967

Table 2. Results of Joint Fits to Magnetic Relaxation Dispersion Profiles from Apo and Holo Gel Samples[a]

	^{2}H		^{17}O	
parameter (unit)	apo	holo	apo	holo
ξ_H	7.6 ± 0.2		9.2 ± 0.3	
$\tau_{S,1}$ (ns)	7.9 ± 0.4		8.4 ± 0.4	
$N_1\,\mathcal{S}_1^2$	4.0 ± 0.2		6.0 ± 0.2	
$\tau_{S,2}$ (ns)	113 ± 5	141 ± 5	[113][b]	[141][b]
N_2			2.6 ± 0.1	4.8 ± 0.2
$N_2\,\mathcal{S}_2^{2\,c}$	0.88 ± 0.02	1.36 ± 0.02	2.6 ± 0.1	4.8 ± 0.2
$\tau_{S,3}$ (μs)	6.1 ± 0.7			
N_3	1.6 ± 0.2	2.5 ± 0.3		
S_3	1.00 ± 0.02			
η_3	0.23 ± 0.06			
$N_3^{\mathrm{eff}}\mathcal{S}_3^{2\,d}$	1.6 ± 0.2	2.4 ± 0.3	0.8 ± 0.1	1.3 ± 0.2
$N_2\,\mathcal{S}_2^2 + N_3^{\mathrm{eff}}\mathcal{S}_3^2$	2.4 ± 0.2	3.8 ± 0.3	3.4 ± 0.2	6.0 ± 0.3
χ^2_{red}	1.3		1.9	

[a]Quoted errors correspond to one standard deviation. [b]Values in square brackets were fixed during the fit. [c]For ^{2}H, $N_2\,\mathcal{S}_2^2$ was obtained directly from the fit. For ^{17}O, $N_2\,\mathcal{S}_2^2$ was computed from eq 5 with the general EMOR model parameters N_2, $S_2 = 1$, and $\eta_2 = 1$. [d]For ^{17}O, the effective solution amplitude parameter $N_3^{\mathrm{eff}}\mathcal{S}_3^2$ was computed from eqs 3 and 5 with N_3 and $\tau_{S,3}$ from the corresponding ^{2}H fit, $S_3 = 1$, and $\eta_3 = \eta_0 = 0.93$.

to have the same values for the apo and holo forms since their tertiary structures are nearly identical.[6,8]

Component 1, here with MST $\tau_{S,1}$ = 7.9 ± 0.4 ns and amplitude parameter $N_1\mathcal{S}_1^2 = 4.0 \pm 0.2$, is invariably found for cross-linked proteins but not for proteins in solution.[34,35] The parameter values obtained for rIFABP are similar to those found for other proteins: $\tau_{S,1}$ = 6.8 ± 0.8 ns and $N_1\mathcal{S}_1^2 = 2.4 \pm 0.2$ for BPTI[34,44] and $\tau_{S,1}$ = 6 ± 1 ns and $N_1\mathcal{S}_1^2 = 3.6 \pm 0.6$ for myoglobin.[35] As before,[34,35] we attribute component 1 chiefly to interfacially confined water molecules in the dense protein clusters of the spatially heterogeneous gel.[39] From component 0 we obtain the dynamic perturbation factor $\xi_H = 7.6 \pm 0.2$, not significantly different from BPTI (7.8 ± 0.3)[34,44] or myoglobin (7.3 ± 0.5).[35] Because some of the cross-linked protein molecules approach closely,[39] ξ_H is larger in the gel than in solution.[41] Solution MRD studies of rIFABP reveal a dispersion component with MST ≈ 1 ns[26,27] (see also Section 3.2), which has been attributed to water exchange among hydration sites in the binding cavity[27] and to exchange of part of the cavity water with external water.[26] Because the 1 ns component cannot be resolved in the gel MRD profiles, it is subsumed in component 1, and this may account for the slightly larger $N_1\mathcal{S}_1^2$ value found for rIFABP as compared to BPTI and myoglobin.

Dispersion components 2 and 3 are responsible for the frequency dependence of R_1 below ∼3 MHz and together account for ∼90% of the excess (over bulk water) R_1 on the low-frequency plateau (Supporting Information, Figure S3). This low-frequency limit is henceforth referred to as $R_1(0)$. For component 2, the holo form has a longer MST (141 vs 113 ns) and a larger amplitude (1.36 vs 0.88) than the apo form. For component 3, only N_3 showed a significant difference between apo and holo so, in the final fit, the remaining parameters $\tau_{S,3}$, S_3, and η_3 were regarded as common to the two forms. We thus find a common MST $\tau_{S,3}$ = 6.1 μs and an occupancy N_3 that is significantly larger in the holo form (2.5 vs 1.6). The order parameters S_3 = 1.00 and η_3 = 0.23 (not far from η_0) indicate that the water molecules responsible for component 3 are highly ordered.

In principle, both internal water molecules and labile deuterons (LDs) in the protein's side chains can contribute to the ^{2}H gel dispersion,[34,35] but the MSTs for component 2 are an order of magnitude too short to be associated with LDs. Only LDs in carboxyl or imidazole groups can exchange sufficiently rapidly, with MSTs in the μs range, to contribute to the ^{2}H profile of cross-linked proteins.[34,35] However, all carboxyl groups of rIFABP are likely to be fully ionized at pD 7.0. Furthermore, rIFABP contains only one His residue and μs LD exchange from such groups can only occur by internal catalysis in a His^+-His or His^+-COO^- pair.[35] We therefore conclude that dispersion components 2 and 3 are both caused entirely by internal water molecules.

The largest contribution to $R_1(0)$ comes from component 3 (Supporting Information, Figure S3), which is in the slow-exchange regime at 27 °C ($\tau_{S,3} > 1/\omega_Q \approx 1$ μs). If the other parameters of component 3 are constant, its contribution is expected to be smaller at lower temperatures,[34,37] where $\tau_{S,3}$ should be even longer. However, we find that $R_1(0)$ increases, monotonically and substantially, as the temperature is reduced first to 15 °C and then to 4 °C (Supporting Information, Figure S7). Global fits to the multitemperature data set show that these observations can be reconciled if component 2, which makes the second largest contribution to $R_1(0)$ at 27 °C (Supporting Information, Figure S3), has a much stronger temperature dependence than component 3. Specifically, if the MSTs are assumed to obey the Arrhenius law and if all other parameters are independent of temperature (a questionable assumption), the global fit suggests activation energies of ∼80 kJ mol^{-1} for $\tau_{S,2}$ and ≲20 kJ mol^{-1} for $\tau_{S,3}$. However, these apparent activation energies should be regarded with caution since they may be influenced by a temperature dependence in the structure or flexibility of the protein.

In the so-called ultraslow-motion limit, where $\omega_Q\,\tau_{S,k} \gg 1$, R_1^k is proportional to $N_k/\tau_{S,k}$ (with no other dependence on $\tau_{S,k}$).[37] Because component 3 is not far from this limit, the parameters N_3 and $\tau_{S,3}$ are sensitive to experimental errors in R_1 at low frequencies. While the MRD data rule out a signficantly smaller $\tau_{S,3}$ value, say 2 μs, fits with $\tau_{S,3}$ fixed to a value larger than 6 μs are nearly as good as the best fit shown in Figure 2. The N_3

DOI: 10.1021/acs.jpcb.5b03214
J. Phys. Chem. B 2015, 119, 7957−7967

value is then increased by approximately the same factor. Therefore, the real uncertainty in N_3 and $\tau_{S,3}$ is signifcantly larger than indicated in Table 2. On the other hand, larger values of N_3 are more difficult to reconcile with other available information (see Section 4).

Figure 3 shows the water ^{17}O MRD profiles obtained at 27 °C from the apo and holo rIFABP gel samples. Within the

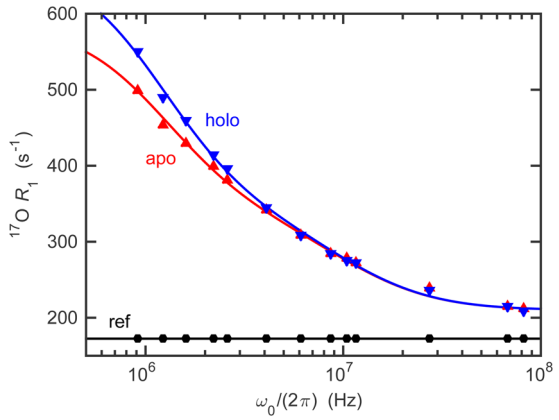

Figure 3. Water ^{17}O MRD profiles from apo (▲) and holo (▼) rIFABP gels at 27.0 °C. Reference sample R_1 values are also shown (●). The two curves resulted from a joint fit to both profiles with the model parameters given in Table 2

MHz frequency range accessible with the ^{17}O nuclide, the contribution from component 3, with MST of 6.1 μs, does not exceed the experimental error in R_1. Two dispersive components should therefore suffice to model the ^{17}O profiles. However, $\tau_{S,2}$ cannot be reliably determined since component 2 does not reach its low-frequency plateau at the lowest ^{17}O frequency of ∼1 MHz (Supporting Information, Figure S4). But the ^{17}O and ^{2}H profiles were measured on the same samples, so the correlation times should be the same. Accordingly, we fix $\tau_{S,2}$ to the values deduced from the ^{2}H fits. Component 2 now requires four parameters since it is not in the fast-exchange (or motional-narrowing) regime for ^{17}O, as it is for ^{2}H. Fits with adjustable order parameter S_2 and fixed η_2 = 0 or 1 do not indicate a significant departure from the high-order limit, S_2 = 1. In the final fit, we therefore enforced S_2 = 1 and chose the option η_2 = 1 consistent with high order (see Section 2.3).

We now compare the parameter values deduced from the ^{17}O profiles with the corresponding ^{2}H values (Table 2). Among the three parameters associated with external hydration water, only $N_1\mathcal{S}_1^2$ differs markedly, being 50% larger in the ^{17}O case. A similar difference, but even more pronounced, is seen for the amplitude parameter $N_2\mathcal{S}_2^2$ of component 2. The only plausible explanation of these differences is that anisotropic internal motions reduce the order parameter $\mathcal{S}$ more for ^{2}H than for ^{17}O.

Even if the internal water molecules responsible for component 2 are highly ordered, they may well undergo 180° flips about the molecular symmetry (C_2) axis during their >100 ns MST in the hydration site. Such C_2 flips do not affect ^{17}O relaxation,[32] but they may alter ^{2}H relaxation in two ways if the mean waiting time between flips τ_{flip} is short compared to the MST.[37] First, there is a direct relaxation contribution from the flip motion. For the concentration normalization used in Figure 2, $R_1^{flip}(0) \approx 6.5(\tau_{flip}/\mu s)^{37}$ so that, with $\tau_{flip} < 0.1$ μs, this contribution is at most comparable to the experimental R_1 error. More importantly, C_2 flips alter the order parameters[37] S and η so that, if no other internal motions occur, $S = -0.555$ and $\eta = 0.718$ and, by way of eq 5, $\mathcal{S}^2 = 0.36$. With C_2 flips as the only internal motion, so that $\mathcal{S}^2 = 1$ for ^{17}O, we thus predict that $N_2\mathcal{S}_2^2(^2H)/N_2\mathcal{S}_2^2(^{17}O) = 0.36$. According to the results in Table 2, this ratio is 0.34 ± 0.02 for apo and 0.28 ± 0.02 for holo. We therefore conclude that the internal water molecules responsible for component 2 undergo C_2 flips during their MST but are otherwise highly ordered. The larger number of water molecules responsible for component 1 are not likely to be as highly ordered as those in component 2, but C_2 flips of some of these water molecules might also explain the ^{2}H/^{17}O difference in $N_1\mathcal{S}_1^2$ (see also Section 3.2).

3.2. Solution Magnetic Relaxation Dispersion Profiles.

^{2}H and ^{17}O MRD profiles from rIFABP solutions have been reported before,[26] but to reliably compare gel and solution MRD data both should be measured on samples made from the same protein preparation and with water of the same isotopic composition. Also, in the previous MRD study of rIFABP,[26] the FA content of the apo and holo samples was not independently determined by GC. We therefore remeasured the ^{2}H and ^{17}O MRD profiles from apo and holo rIFABP solution samples (Figures 4 and 5).

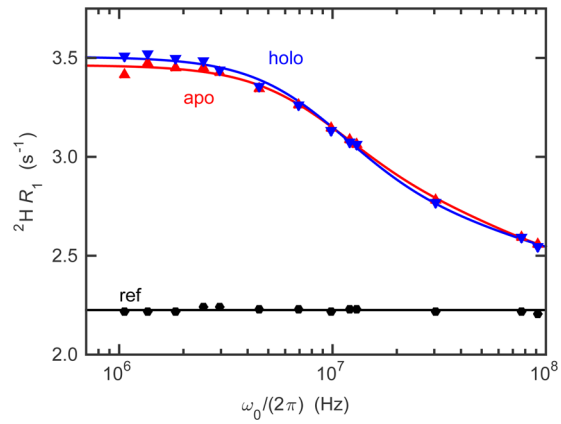

Figure 4. Water ^{2}H MRD profiles from apo (▲) and holo (▼) rIFABP solutions at 27.0 °C. Reference sample R_1 values are also shown (●). The two curves resulted from a joint fit to both profiles with the model parameters given in Table 3.

The solution profiles provide information about the 1 ns component, which is obscured by the much larger gel-induced 8 ns component in the gel profiles (for simplicity, we refer to both as component 1). Because the 1 ns dispersion is centered near the high-frequency end of the ^{17}O profile, its two parameters cannot be determined with useful accuracy without fixing the dynamic perturbation factor of the external hydration shell. We therefore set ξ_H = 4.2, the mean value obtained for 11 proteins at 27 °C.[41,45] To reduce the covariance in the parameters of the overlapping components 1 and 2 (Supporting Information, Figures S5 and S6), we fix the longer correlation time to $\tau_{C,2}$ = 7.7 ns, which is the isotropic rotational correlation time τ_R of rIFABP at 27 °C, corrected for the viscosity of our water isotope mixture.[26] Solution component 2 is produced by the water molecules responsible for gel components 2 and 3, which all have MSTs much longer than

DOI: 10.1021/acs.jpcb.5b03214
J. Phys. Chem. B 2015, 119, 7957−7967

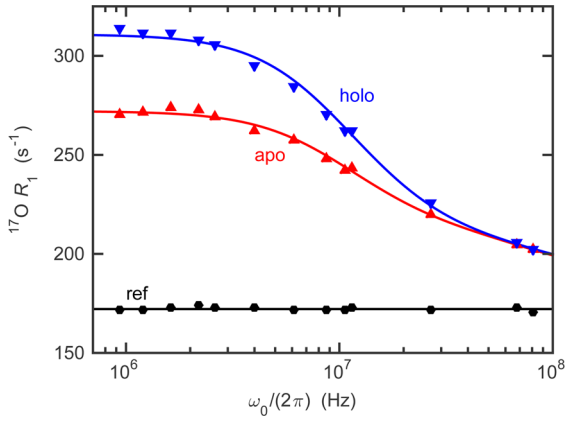

Figure 5. Water ^{17}O MRD profiles from apo (▲) and holo (▼) rIFABP solutions at 27.0 °C. Reference sample R_1 values are also shown (●). The two curves resulted from a joint fit to both profiles with the model parameters given in Table 3.

τ_R (Table 2). We therefore expect that $\tau_{C,2} = \tau_R$ (see Section 2.3).

The results of the joint fits in Figures 4 and 5 are presented in Table 3. Component 1 has an MST of ~1.1 ns for apo and ~0.6 ns (but with a large uncertainty) for holo. The difference is barely significant, but it emerges consistently from both the ^2H and ^{17}O data. The amplitude parameter $N_1\,\mathcal{S}_1^2$ can only be accurately determined for the apo form, but the data are consistent with the same value for the holo form. The value of $N_1\,\mathcal{S}_1^2$ represents a lower bound (since $\mathcal{S}_1^2 \leq 1$) on the number of water molecules responsible for component 1. The insignificant $^2H/^{17}O$ difference in $N_1\,\mathcal{S}_1^2$ indicates that C_2 flips hardly occur on the sub-nanosecond time scale. We caution, however, that $N_1\,\mathcal{S}_1^2$ depends on the assumed ξ_H value. Varying ξ_H from 3.6 (as for the small protein BPTI[41]) to 5.8 (as for myoglobin[35]), we find (from fits of similar quality) that $N_1\,\mathcal{S}_1^2$ varies from ~12 to ~4, while $\tau_{S,1}$ varies over the range 0.5–2.1 ns.

Table 3. Results of Joint Fits to Magnetic Relaxation Dispersion Profiles from Apo and Holo Solution Samples[a]

	^2H		^{17}O	
parameter (unit)	apo	holo	apo	holo
ξ_H	[4.2][b]		[4.2][b]	
$\tau_{S,1}$ (ns)	1.2 ± 0.1	0.6 ± 0.4	1.0 ± 0.2	0.6 ± 0.6
$N_1\,\mathcal{S}_1^2$	8.8 ± 0.6	9 ± 9	11 ± 2	12 ± 12
$\tau_{C,2}$ (ns)	[7.7][b]		[7.7][b]	
$N_2^{eff}\mathcal{S}_2^{2\,c}$	3.0 ± 0.2	4.2 ± 0.2	3.0 ± 0.2	9.0 ± 0.5
χ^2_{red}	1.3		0.8	

[a]Quoted errors correspond to one standard deviation. [b]Values in square brackets were fixed during the fit. [c]Effective amplitude parameter in the sense of eq 3.

The amplitude parameter $N_2^{eff}\mathcal{S}_2^2$ of component 2 is virtually unaffected by the ξ_H value. This is an effective parameter in the sense of eq 3, because all internal water molecules that contribute to component 2 are not necessarily in the fast-exchange limit. Specifically, whereas gel component 3 does not contribute significantly to the ^{17}O gel profile, it does contribute partially to the ^{17}O solution profile. If the internal water molecules responsible for gel components 2 and 3 also account for solution component 2, then the combined (effective) amplitude parameter derived from the gel profiles (given in the penultimate row of Table 2) should match the $N_2^{eff}\mathcal{S}_2^2$ values in Table 3.

For ^2H, the effective amplitude parameters derived from the solution profiles are similar to, but slightly larger than, the corresponding values derived from the gel profiles. The most likely origin of this difference is an LD contribution to the solution profiles. The difference, ~0.5 D_2O equivalents, corresponds to at least one LD and more if the LD order parameter is <1. Although most of the LDs in the 18 hydroxyl groups, 15 lysine, and 6 arginine side chains should exchange on the millisecond time scale at pD 7.4,[46−48] a few LDs may well have MSTs in the range of a few 100 μs required to contribute to the solution ^2H profiles.

For ^{17}O, the effective amplitude parameters from the gel and solution profiles match reasonably well for apo, but for holo the solution parameter is 50% larger than the gel parameter. This finding can be explained if, in the holo form, several internal water molecules have MSTs on the order of 10 ns. While such water molecules would contribute to solution component 2, they would be subsumed in gel component 1. Moreover, if these water molecules undergo fast C_2 flips, the corresponding solution/gel difference for ^2H would be ~threefold smaller (see Section 3.1). Consistent with this explanation, the amplitude parameter for gel component 1 is 50% larger for ^{17}O than for ^2H (Table 2).

4. DISCUSSION

The MRD analysis presented here allows us to characterize internal water dynamics in apo and holo rIFABP in greater detail and on a far wider range of time scales than previously possible.[20,26−28] On the basis of MRD studies of numerous proteins, it can safely be concluded that all water molecules found here with MSTs exceeding ~10 ns are located in the binding cavity or are buried elsewhere in the protein. But the precise locations of these trapped water molecules are not directly evident from the MRD results. In the following, we present a synthesis of the dynamic information obtained here and structural and mechanistic information deduced from X-ray crystallography and MD simulations. Unless otherwise noted, we use labels from the apo rIFABP structure 1IFC[6] when referring to specific hydration sites.

4.1. Water Exchange (6 μs) and Gap Fluctuations. We consider first the most long-lived (6 μs MST) and highly ordered ($S \approx 1$, $\eta \approx \eta_0$) hydration sites, with occupancy 1.6 in apo and 2.5 in holo (Table 2). The most obvious candidate site with these characteristics is w135, occupied by a highly conserved and highly ordered water molecule H-bonded to three backbone atoms in the βD−βE loop (Figure 1).[5−8,20,22,23,26−28] This site is located inside the β-barrel but not in the lipid-binding cavity. Because the occupancies are nonintegral, at least one 6 μs hydration site must either be partially occupied or have a widely different MST (or even not exist) in some members of the native-state conformational ensemble. The rIFABP crystal structures locate a few hydration sites (such as w217) in deep pockets on the external protein surface, but both MRD studies of other cross-linked proteins[34,35] and the 5 ns MD simulation of rIFABP[20] suggest much shorter MSTs for such surface pockets.

DOI: 10.1021/acs.jpcb.5b03214
J. Phys. Chem. B 2015, 119, 7957−7967

The additional (apart from w135) 6 μs sites are more likely to be found in deep pockets at the periphery of the irregularly shaped binding cavity. The strongest candidate is w152 in the βC−βD loop, occupied by the second (after w135) or third most highly ordered water molecule in the crystal structure[6] and in the MD simulation.[20] The water molecule in site w135 is essential for maintaining the position in the β-barrel of strands D and E (whose backbones are not linked by any direct H-bonds).[6,22] The release of water w135 may therefore be coupled to a large-scale conformational fluctuation that further opens the gap between β-strands D and E. This fluctuation might also disrupt site w152 at the other end of the βD strand, accounting for the common MST of these two water molecules. While smaller openings of the gap that allow other cavity water molecules to escape may occur more frequently (see Section 4.3), the 6 μs fluctuation is thought to be more extensive and may even allow the FA to enter or leave the cavity. The additional 6 μs water required to account for the higher occupancy in the holo form may be the water molecule (site w170 in the myristate- and palmitate-rIFABP structures 1ICM and 2IFB) that donates strong H-bonds to the charged carboxylate oxygens of Glu51 and the FA headgroup near the βD−βE gap.[5,7,8] This location would account for the common MST and the strong H-bonds would make the C_2 flip of this water very slow, as required by the large ^{2}H order parameter.

4.2. Water Exchange (~100 ns) and Portal Fluctuations. The second most long-lived hydration sites, with MST 113 versus 141 ns, have occupancy 2.6 versus 4.8 in the apo and holo forms, respectively (Table 2). While highly ordered ($\mathcal{S}^2(^{17}\mathrm{O}) \approx 1$), the water molecules in these sites undergo C_2 flips ($\mathcal{S}^2(^2\mathrm{H}) \approx 0.3$). On the basis of these characteristics, the possible locations for these sites are in the binding cavity and/or in deep pockets on the external protein surface. But the substantial increase of the occupancy upon palmitate binding indicates that most, if not all, of these sites are located in the binding cavity. Apart from displacing some of the cavity waters, the bound FA constricts the portal opening, which in the apo form is wide enough to allow water molecules to pass through, and blocks the remaining orifice by its terminal methyl group.[5,7,8] The 4.8 occupancy of the holo form may therefore refer to some of the six cavity waters identified in palmitate-rIFABP crystal structure.[5] Consistent with the high orientational order inferred from the MRD data, these water molecules have high positional order: their average crystallographic B factor is only 9% larger than the average B factor for all protein atoms,[5] compared to 134% for the apo form.[7] If this assignment is correct, the 141 ns MST likely corresponds to the opening frequency of the portal in the holo form. Portal fluctuations on this time scale may control the exchange of a few cavity waters, but they cannot be rate-limiting for the much slower FA dissociation.[18]

The 2.6 apo occupancy does not necessarily correspond to a subset of the hydration sites responsible for the 4.8 holo occupancy. Long-lived hydration sites may be created (through portal blocking) as well as eliminated (through displacement) by the bound FA. The apo hydration sites may be some of the five crystallographically identified water-occupied pockets in the periphery of the binding cavity, which might be disrupted by conformational fluctuations in the portal region occurring on a similar time scale as the corresponding fluctuations in the holo form (thus accounting for the similar apo and holo MSTs). A less likely possibility is that the apo hydration sites are the ~3 deep water-occupied pockets on the external protein surface. Since these sites are present in both apo and holo forms,[5,7,8] only 2.2 ± 0.2 water molecules would then be gated by the portal in the holo form, and the similar MSTs for hydration sites inside and outside the binding cavity would be coincidental.

4.3. Water Exchange (~1 ns) within and out of the Binding Cavity. Together, the 6 μs and ~100 ns hydration sites account for a water occupancy of 3.2 ± 0.2 (apo) or 6.3 ± 0.4 (holo) in the binding cavity (Table 2, with 1 unit subtracted for w135), significantly less than the total water occupancy N_{cav} of this cavity. MD simulations of rIFABP[20] find substantially more cavity water than what is included in diffraction-based structure models. For apo-rIFABP, N_{cav} = 31.8 according to the simulation,[20] whereas only 22 hydration sites were identified in the 1.2 Å apo structure 1IFC.[7] For palmitate-rIFABP, the simulation[20] yields N_{cav} = 19.7, as opposed to six and eight hydration sites, respectively, in the 2.0 Å palmitate-rIFABP structure 2IFB[8] and the 1.5 Å myristate-rIFABP structure 1ICM.[5] (These N_{cav} values do not include w135.) Similarly large discrepancies between simulation and crystallography are found for chicken liver bile acid-binding protein (N_{cav} = 30 from simulation[29] for both apo and holo vs N_{cav} = 21 (apo) and 13 (holo) from crystallography[30]) and human heart-type FABP (N_{cav} = 26 from simulation[31] vs 13 from crystallography for the holo form). In all cases, the simulations found large fluctuations in N_{cav}, implying a substantial positional disorder for at least some of the hydration sites, which would make these sites difficult to detect by X-ray diffraction.

Adopting the simulated N_{cav} values and subtracting the occupancies for the 6 μs and ~100 ns hydration sites, we can estimate the mean-square order parameter for the ~1 ns cavity water from the $N_1\,\mathcal{S}_1^2$ values in Table 3. Using the ^{2}H data (the ^{17}O data yield similar results but with larger errors), we thus obtain $\mathcal{S}^2 = 0.3$ for apo and $\mathcal{S}^2 = 0.7$ for holo. Although the latter value has a large uncertainty, it thus appears that the mobile cavity waters are more highly ordered in the holo form than in the apo form. This would be consistent with the smaller positional disorder (as gauged by the B factor) for the apo waters in the crystal structures (see above) and in the simulation.[20] If we had used a different fixed ξ_H value when fitting the solution MRD profiles, we would have obtained different $\mathcal{S}^2$ values (see above), but the $\mathcal{S}^2$(apo)/$\mathcal{S}^2$(holo) ratio would be the same. We therefore conclude that the similarity of the $N_1\,\mathcal{S}_1^2$ values for apo and holo (Table 3) is a fortuitous result: the smaller water occupancy (N_1) of the holo cavity is compensated by the higher order ($\mathcal{S}_1^2$) of these water molecules.

According to this interpretation, the ~1 ns MST pertains to most of the cavity water (28.6 water molecules in the apo cavity, 13.4 in the holo cavity). But the mechanistic interpretation of the MST raises several questions. Does this MST refer to water exchange out of the binding cavity[26] or to water exchange among different hydration sites within the cavity?[27] In the former case, which pathway is used (portal, gate, and/or backside portal), and what is the rate-limiting factor (conformational gating or escape from the hydration site)? In the latter case, how and on what time scale do these water molecules eventually escape from the cavity?

In the apo form, the portal has a wide opening,[7] and NMR indicates backbone disorder in this region.[10] Water molecules

DOI: 10.1021/acs.jpcb.5b03214
J. Phys. Chem. B 2015, 119, 7957−7967

residing near the portal may thus exchange directly from the cavity on an ~1 ns time scale. But in the holo form the portal is blocked by the palmitate tail,[5] so water exchange via this pathway should be much slower. Since we find a slightly shorter MST for holo than for apo (0.6 vs 1.1 ns), the ~1 ns component cannot be dominated by exchange via the portal. In the 5 ns rIFABP simulation, water exchanged from the apo cavity mainly via the portal and backside portal and from the holo cavity mainly via the portal and gap.[20] But the palmitate headgroup was displaced by ~6 Å from its crystallographic position, so the portal may not have been obstructed in the simulated holo protein. In the simulation, 24 (apo) and 6 (holo) water molecules remained in the binding cavity throughout the trajectory,[20] indicating that these water molecules have MSTs ≫ 5 ns. To be consistent with this result, the MRD-derived ~1 ns MST must refer mainly to intracavity site exchange. While most cavity waters must visit several hydration sites before they can escape from the cavity, direct exchange with external water might occur on the same time scale from a few hydration sites near the portal, gap, or backside portal. Intracavity exchange may not average out the anisotropic nuclear quadrupole coupling completely, but the residual anisotropy may be so small that it does not affect the MRD profile significantly.[27]

5. CONCLUSIONS

To characterize internal-water exchange and associated conformational dynamics in rIFABP, we recorded the water ^{2}H and ^{17}O MRD profiles for the apo and palmitate-bound forms. MRD measurements were performed on freely tumbling rIFABP in dilute solution as well as on immobilized rIFABP in covalently cross-linked gels. The gel samples allowed us to directly determine internal-water exchange times (or MSTs) as long as 10^{-5} s from ^{2}H MRD profiles extending over five decades of magnetic field strength (or NMR frequency).

The extensive MRD data set was analyzed with the general and accurate EMOR relaxation theory, allowing us to extract the water occupancy N, the mean-square order parameter $\mathcal{S}^2$, and the MST τ_S values for three dynamically resolved classes of hydration sites. By interpreting the MRD results in the light of structural knowledge gleaned from crystallography and MD simulations, we arrive at the following consistent scenario of dynamic processes in the binding cavity of rIFABP (at 27 °C).

(1) Most of the water molecules trapped in the lipid binding cavity (90% for apo, 70% for holo) exchange among well-defined hydration sites on a time scale of ~1 ns, 3 orders of magnitude slower than in bulk water. Because they are extensively H-bonded, these water molecules experience orientational constraints, more so in the tighter holo cavity ($\mathcal{S}^2 \approx 0.7$) than for the larger water cluster in the apo cavity ($\mathcal{S}^2 \approx 0.3$). Water molecules residing near transient or permanent cavity openings, such as the portal in the apo form, exchange with external water on the same ~1 ns time scale.

(2) A small number of cavity waters (2.6 for apo, 4.8 for holo) are trapped for ~100 ns (110 ns for apo, 140 ns for holo) before escaping from the binding cavity. At least for the holo form, the exchange of these water molecules may be gated by large-scale fluctuations of the portal and/or the bound FA. These water molecules exhibit high orientational order but undergo C_2 flips while residing in their hydration sites.

(3) The longest motional time scale revealed by the MRD data, ~6 μs, is associated with a major widening of the gap between β-strands D and E. This motion releases the 2 (apo) or 3 (holo) most long-lived and highly ordered internal water molecules in the rIFABP structure. Two of these reside in small pockets in the loops at either end of the βD strand, the third one interacts with the FA headgroup.

(4) The opening rates for the portal and gap are orders of magnitude faster than FA dissociation. The escape of a few structurally important water molecules, but not the dissociation of the FA ligand, is rate-limited by fluctuations of these gates.

■ ASSOCIATED CONTENT

Supporting Information

Two figures with results of the GC analysis, four figures showing the individual components of all MRD profiles, and one figure showing ^{2}H MRD profiles for the apo and holo gel samples at four temperatures. The Supporting Information is available free of charge on the ACS Publications website at DOI: 10.1021/acs.jpcb.5b03214.

■ AUTHOR INFORMATION

Corresponding Authors

*E-mail: kaieda.shuji@gmail.com. (S.K.)
*E-mail: bertil.halle@bpc.lu.se. (B.H.)

Notes

The authors declare no competing financial interest.

■ ACKNOWLEDGMENTS

We thank I. Ropson (Pennsylvania State Univ.) for advice on rIFABP expression, A. Rogstam (Lund Protein Production Platform) for rIFABP preparation, J. Mangas and P. Adlercreutz (Dept. of Biotechnology, Lund Univ.) for help with gas chromatography experiments, and the Swedish Research Council and the Royal Physiographic Society in Lund for financial support.

■ REFERENCES

(1) Zimmerman, A. W.; Veerkamp, J. H. New Insights into the Structure and Function of Fatty Acid-Binding Proteins. *Cell. Mol. Life Sci.* **2002**, *59*, 1096−1116.
(2) Storch, J.; Thumser, A. E. Tissue-Specific Functions in the Fatty Acid-Binding Protein Family. *J. Biol. Chem.* **2010**, *285*, 32679−32683.
(3) Smathers, R. L.; D. R. Petersen, D. R. The Human Fatty Acid-Binding Protein Family: Evolutionary Divergences and Functions. *Hum. Genomics* **2011**, *5*, 170−191.
(4) Marcelino, A. M. C.; Smock, R. G.; Gierasch, L. M. Evolutionary Coupling of Structural and Functional Sequence Information in the Intracellular Lipid-Binding Protein Family. *Proteins* **2006**, *63*, 373−384.
(5) Sacchettini, J. C.; Gordon, J. I.; Banaszakl, L. J. Crystal Structure of Rat Intestinal Fatty-Acid-Binding protein: Refinement and Analysis of the *Escherichia coli*-Derived Protein with Bound Palmitate. *J. Mol. Biol.* **1989**, *208*, 327−339.
(6) Scapin, G.; Gordon, J. I.; Sacchettini, J. C. Refinement of the Structure of Recombinant Rat Intestinal Fatty Acid-Binding Apoprotein at 1.2-Å Resolution. *J. Biol. Chem.* **1992**, *267*, 4253−4269.
(7) Sacchettini, J. C.; Scapin, G.; Gopaul, D.; Gordon, J. I. Refinement of the Structure of *Escherichia coli*-derived Rat Intestinal Fatty Acid Binding Protein with Bound Oleate to 1.75-Å Resolution. *J. Biol. Chem.* **1992**, *267*, 23534−23545.

DOI: 10.1021/acs.jpcb.5b03214
J. Phys. Chem. B 2015, 119, 7957−7967

(8) Eads, J.; Sacchettini, J. C.; Kromminga, A.; Gordon, J. I. *Escherichia coli*-Derived Rat Intestinal Fatty Acid Binding Protein With Pound Myristate at 1.5Å Resolution and I-FABP$^{Arg106\rightarrow Gln}$ with Bound Oleate at 1.74Å Resolution. *J. Biol. Chem.* **1993**, *268*, 26375−26385.
(9) Hodsdon, M. E.; Ponder, J. W.; Cistola, D. P. The NMR Solution Structure of Intestinal Fatty Acid-Binding Protein Complexed with Palmitate: Application of a Novel Distance Geometry Algorithm. *J. Mol. Biol.* **1996**, *264*, 585−602.
(10) Hodsdon, M. E.; Cistola, D. P. Discrete Backbone Disorder in the Nuclear Magnetic Resonance Structure of Apo Intestinal Fatty Acid-Binding Protein: Implications for the Mechanism of Ligand Entry. *Biochemistry* **1997**, *36*, 1450−1460.
(11) Cistola, D. P.; Kim, K.; Rogl, H.; Frieden, C. Fatty Acid Interactions with a Helix-Less Variant of Intestinal Fatty Acid-Binding Protein. *Biochemistry* **1996**, *35*, 7559−7565.
(12) Corsico, B.; Cistola, D. P.; Frieden, C.; Storch, J. The Helical Domain of Intestinal Fatty Acid Binding Protein is Critical for Collisional Transfer of Fatty Acids to Phospholipid Membranes. *Proc. Natl. Acad. Sci. U.S.A.* **1998**, *95*, 12174−12178.
(13) Falomir-Lockhart, L. J.; Laborde, L.; Kahn, P. C.; Storch, J.; Córsico, B. Protein-Membrane Interaction and Fatty Acid Transfer from Intestinal Fatty Acid-Binding Protein to Membranes. Support for a Multistep Process. *J. Biol. Chem.* **2006**, *281*, 13979−13989.
(14) Mihajlovic, M.; Lazaridis, T. Modeling Fatty Acid Delivery from Intestinal Fatty Acid Binding Protein to a Membrane. *Protein Sci.* **2007**, *16*, 2042−2055.
(15) Friedman, R.; Nachliel, E.; Gutman, M. Molecular Dynamics Simulations of the Adipocyte Lipid Binding Protein Reveal a Novel Entry Site for The Ligand. *Biochemistry* **2005**, *44*, 4275−4283.
(16) Levin, L. B. A.; Nachliel, E.; Gutman, M.; Tsfadia, Y. Molecular Dynamics Study of the Interaction between Fatty Acid Binding Proteins with Palmitate Mini-Micelles. *Mol. Cell. Biochem.* **2009**, *326*, 29−33.
(17) Long, D.; Mu, Y.; Yang, D. Molecular Dynamics Simulation of Ligand Dissociation from Liver Fatty Acid Binding Protein. *PLoS One* **2009**, *4*, e6081.
(18) Richieri, G. V.; Low, P. J.; Ogata, R. T.; Kleinfeld, A. M. Binding Kinetics of Engineered Mutants Provide Insight about the Pathway for Entering and Exiting the Intestinal Fatty Acid Binding Protein. *Biochemistry* **1999**, *38*, 5888−5895.
(19) Long, D.; Yang, D. Millisecond Timescale Dynamics of Human Liver Fatty Acid Binding Protein: Testing of Its Relevance to the Ligand Entry Process. *Biophys. J.* **2010**, *98*, 3054−3061.
(20) Bakowies, D.; van Gunsteren, W. F. Simulations of Apo and Holo-Fatty Acid Binding Protein: Structure and Dynamics of Protein, Ligand and Internal Water. *J. Mol. Biol.* **2002**, *315*, 713−736.
(21) Bakowies, D.; van Gunsteren, W. F. Water in Protein Cavities: A Procedure to Identify Internal Water and Exchange Pathways and Application to Fatty Acid-Binding Protein. *Proteins* **2002**, *47*, 534−545.
(22) Likić, V. A.; Juranić, N.; Macura, S.; Prendergast, F. G. A "Structural" Water Molecule in the Family of Fatty Acid Binding Proteins. *Protein Sci.* **2000**, *9*, 497−504.
(23) Bottoms, C. A.; White, T. A.; Tanner, J. J. Exploring Structurally Conserved Solvent Sites in Protein Families. *Proteins* **2006**, *64*, 404−421.
(24) Ropson, I. J.; Frieden, C. Dynamic NMR Spectral Analysis and Protein Folding: Identification of a Highly Populated Folding Intermediate of Rat Intestinal Fatty Acid-Binding Protein by ^{19}F NMR. *Proc. Natl. Acad. Sci. U.S.A.* **1992**, *89*, 7222−7226.
(25) Kim, K.; Frieden, C.; Ramanathan, R. Intestinal Fatty Acid Binding Protein: A Specific Residue in One Turn Appears To Stabilize the Native Structure and Be Responsible for Slow Refolding. *Protein Sci.* **1997**, *6*, 364−372.
(26) Wiesner, S.; Kurian, E.; Prendergast, F. G.; Halle, B. Water Molecules in the Binding Cavity of Intestinal Fatty Acid Binding Protein: Dynamic Characterization by Water ^{17}O and ^{2}H Magnetic Relaxation Dispersion. *J. Mol. Biol.* **1999**, *286*, 233−246.
(27) Modig, K.; Rademacher, M.; Lücke, C.; Halle, B. Water Dynamics in the Large Cavity of Three Lipid-Binding Proteins Monitored by ^{17}O Magnetic Relaxation Dispersion. *J. Mol. Biol.* **2003**, *332*, 965−977. In eqs S11 and S14 of the Supporting Information, τ_C^{loc} should be replaced by $\exp(-\tau/\tau_C^{loc})$.
(28) Likić, V. A.; Prendergast, F. G. Dynamics of Internal Water in Fatty Acid Binding Protein: Computer Simulations and Comparison with Experiments. *Proteins* **2001**, *43*, 65−72.
(29) Ricchiuto, P.; Rocco, A. G.; Gianazza, E.; Corrada, D.; Beringhelli, T.; Eberini, I. Structural and Dynamic Roles of Permanent Water Molecules in Ligand Molecular Recognition by Chicken Liver Bile Acid Binding Protein. *J. Mol. Recognit.* **2008**, *21*, 347−353.
(30) Nichesola, D.; Perduca, M.; Capaldi, S.; Carrizo, M. E.; Righetti, P. G.; Monaco, H. L. Crystal structure of chicken liver basic fatty acid-binding protein complexed with cholic acid. *Biochemistry* **2004**, *43*, 14072−14079.
(31) Matsuoka, D.; Sugiyama, S.; Murata, M.; Matsuoka, S. Molecular Dynamics Simulations of Heart-Type Fatty Acid-Binding Protein in Apo and Holo Forms, and Hydration Structure Analyses in the Binding Cavity. *J. Phys. Chem. B* **2015**, *119*, 114−127.
(32) Halle, B., Denisov, V. P., Venu, K. Multinuclear Relaxation Dispersion Studies of Protein Hydration In *Biological Magnetic Resonance;* Krishna, N. R., Berliner, L. J., Eds.; Kluwer/Plenum: New York, 1999; Vol. *17* pp 419−484.
(33) Halle, B., Denisov, V. P., Modig, K., Davidovic, M. Protein Conformational Transitions As Seen from the Solvent: Magnetic Relaxation Dispersion Studies of Water, Co-Solvent, and Denaturant Interactions with Nonnative Proteins. In *Protein Folding Handbook;* Buchner, J., Kiefhaber, T., Eds.; Wiley-VCH: Weinheim, Germany, 2005; Vol. *I*, Chapter 8, pp 201−246.
(34) Persson, E.; Halle, B. Nanosecond to Microsecond Protein Dynamics Probed by Magnetic Relaxation Dispersion of Buried Water Molecules. *J. Am. Chem. Soc.* **2008**, *130*, 1774−1787.
(35) Kaieda, S.; Halle, B. Internal Water and Microsecond Dynamics in Myoglobin. *J. Phys. Chem. B* **2013**, *117*, 14676−14687.
(36) Halle, B. Spin Dynamics of Exchanging Quadrupolar Nuclei in Locally Anisotropic Systems. *Progr. NMR Spectrosc.* **1996**, *28*, 137−159.
(37) Nilsson, T.; Halle, B. Nuclear Magnetic Relaxation Induced by Exchange-Mediated Orientational Randomization: Longitudinal Relaxation Dispersion for Spin $I = 1$. *J. Chem. Phys.* **2012**, *137*, 54503.
(38) Savitsky, P.; Bray, J.; Cooper, C. D. O.; Marsden, B. D.; Mahajan, P.; Burgess-Brown, N. A.; Gileadi, O. High-Throughput Production of Human Proteins for Crystallization: The SGC Experience. *J. Struct. Biol.* **2010**, *172*, 3−13.
(39) Kaieda, S.; Plivelic, T. S.; Halle, B. Structure and Kinetics of Chemically Cross-Linked Protein Gels from Small-Angle X-Ray Scattering. *Phys. Chem. Chem. Phys.* **2014**, *16*, 4002−4011.
(40) Ferrante, G.; Sykora, S. Technical Aspects of Fast Field Cycling. *Adv. Inorg. Chem.* **2005**, *57*, 405−470.
(41) Mattea, C.; Qvist, J.; Halle, B. Dynamics at the Protein-Water Interface from ^{17}O Spin Relaxation in Deeply Supercooled Solutions. *Biophys. J.* **2008**, *95*, 2951−2963.
(42) Halle, B. The Physical Basis of Model-Free Analysis of NMR Relaxation Data from Proteins and Complex Fluids. *J. Chem. Phys.* **2009**, *131*, 224507.
(43) Coleman, T. F.; Li, Y. An Interior Trust Region Approach for Nonlinear Minimization Subject to Bounds. *SIAM J. Optim.* **1996**, *6*, 418−445.
(44) Persson, F.; Halle, B. Transient Access to the Protein Interior: Simulation versus NMR. *J. Am. Chem. Soc.* **2013**, *135*, 8735−8748.
(45) Halle, B. Protein Hydration Dynamics in Solution: A Critical Survey. *Philos. Trans. R. Soc., B* **2004**, *359*, 1207−1224.
(46) Denisov, V. P.; Halle, B. Hydrogen Exchange and Protein Hydration: The Deuteron Spin Relaxation Dispersions of Bovine Pancreatic Trypsin Inhibitor and Ubiquitin. *J. Mol. Biol.* **1995**, *245*, 698−709.

DOI: 10.1021/acs.jpcb.5b03214
J. Phys. Chem. B 2015, 119, 7957−7967

(47) Liepinsh, E.; Otting, G. Proton Exchange Rates from Amino Acid Side Chains − Implications for Image Contrast. *Magn. Reson. Med.* **1996**, *35*, 30−42.
(48) Vaca Chávez, F.; Hellstrand, E.; Halle, B. Hydrogen Exchange and Hydration Dynamics in Gelatin Gels. *J. Phys. Chem. B* **2006**, *110*, 21551−21559.

DOI: 10.1021/acs.jpcb.5b03214
J. Phys. Chem. B 2015, 119, 7957−7967